PAPER

Check for updates

Synthesis, characterization and antimicrobial activity of ZnO-QDs @ bis MPA polyester-64-hydroxyl dendrimer nanostructures†

Archana Zala [ID] * and Harshad Patel

This study presents the successful synthesis and characterization of five novel zinc oxide quantum dots @ bis MPA polyester-64-hydroxyl dendrimer nanostructures with tuneable hydrophilicity. A unique feature of these ZnO quantum dots @ bis MPA polyester-64-hydroxyl dendrimer nanostructures is the functionalization of the bis MPA polyester-64-hydroxyl dendrimer with five different varying numbers of surface hydroxyl functional groups with zinc oxide quantum dots. The surface groups varied from 1, 5, 10, 20 and 40 zinc oxide quantum dots in ZnO-QDs @ bis MPA polyester-64-hydroxyl dendrimer nanostructures, respectively. The highly water-dispersible ZnO quantum dots @ bis MPA polyester-64-hydroxyl dendrimer nanostructures $G4-R(ZnO-QDs)_1$, $G4-R(ZnO-QDs)_5$, $G4-R(ZnO-QDs)_{10}$, $G4-R(ZnO-QDs)_{20}$ and $G4-R(ZnO-QDs)_{40}$ were chemically synthesized. The ZnO-QDs @ bis MPA polyester-64-hydroxyl dendrimer nanostructures were characterized using techniques such as UV-vis-NIR spectroscopy, atomic force microscopy, dynamic light scattering, attenuated total reflectance Fourier transform infrared spectroscopy, and Raman spectroscopy. Notably, these ZnO quantum dots @ bis MPA polyester-64-hydroxyl dendrimer nanostructures exhibited high water-dispersibility. A significant finding is that the unique feature of ZnO quantum dots @ bis MPA polyester-64-hydroxyl dendrimer nanostructures demonstrated synergistic antibacterial activity against Gram-positive bacteria. This research contributes to the growing field of nanotechnology by providing a method to tune the hydrophilicity, optical properties, molecular vibration, size and toxicity of nanostructures, which could have broad impacts on various scientific and technological domains.

Sustainability spotlight

Few studies have been reported on bis MPA polyester-64-hydroxyl dendrimers, so they are attracting attention for exploring new applications. The bis MPA polyester-64-hydroxyl dendrimers can be pioneers for various applications. Dendrimers are a promising field for exploring new applications. The bis MPA polyester-64-hydroxyl dendrimer is a versatile nanopolymer that can be modified with various surface functional groups to enhance its properties and applications. This study represented the addition of zinc oxide quantum dots in the bis MPA polyester-64-hydroxyl dendrimer with five different amounts of surface functional groups functionalized. The resulting ZnO-QDs @ bis MPA polyester-64-hydroxyl dendrimer nanostructures exhibited unique characteristics and tuneable chemical and physical properties. This work has successfully synthesized five unique ZnO-QDs @ bis MPA polyester-64-hydroxyl dendrimer nanostructures with distinct properties and potential applications. The ZnO-QDs @ bis MPA polyester-64-hydroxyl dendrimer nanostructures have high-water solubility, a complex molecular vibration spectrum, antibacterial activity, and a spherical morphology with variable size and surface roughness.

Introduction

Dendrimers are a newly developed dendritic three-dimensional nano-polymer and have a lot of potential for surface modifications and applications. They are biodegradable and non-toxic, making them ideal materials for use in a variety of fields. The unique structure of dendrimers allows for a high degree of customization, allowing researchers to tailor the properties to suit specific needs. With a combination of versatility and safety, dendrimers are poised to become an important tool in the development of new technologies. The bis MPA polyester-64-hydroxyl dendrimer nanostructures have been reported to be bio-degradable,[1] non-toxic three-dimensional nanostructures with a polyvalent hydroxyl surface functional group. This fourth-generation system is hydrophobic in nature, which potentially restricts its use in biomedical and other applications. Few studies have been reported on the bis MPA polyester-64-hydroxyl dendrimer, so it is attracting attention for exploring new applications. The bis MPA polyester-64-hydroxyl dendrimers can be pioneers for various applications. The

School of Engineering and Technology, National Forensic Sciences University, Gandhinagar, 382 007, Gujarat, India. E-mail: archana.zala@nfsu.ac.in; archanazala3@gmail.com

dendrimers are a promising field for exploring new applications. The bis MPA polyester-64-hydroxyl dendrimer is a versatile nanopolymer that can be modified with various surface functional groups to enhance its properties and applications. The bis MPA polyester-64-hydroxyl dendrimer has sixty-four hydroxyl surface functional groups, which were selectively functionalized with zinc oxide quantum dots at different distinct levels.

Antimicrobial resistance is a phenomenon where microorganisms such as bacteria, viruses, fungi, parasites, and others evolve to become resistant to the antimicrobial agents used to treat infections.[2] Superbugs are germs that have developed resistance to most of antimicrobials.[3] This is a serious issue because a resistant infection can be fatal and infectious for both individuals and society.[3] Antimicrobial resistance encompasses resistance to several types of medication, including antibacterial, antiviral, and antifungal medication.[4] The development of novel biocidal or disinfecting substances to supplement existing antibiotics has become a focus of scientific interest in the fight against illnesses caused by bacteria and its cytolytic toxins. *Staphylococcus aureus* (*S. aureus*) is commonly found in the environment (soil, water and air) and is also found in the nose and on the skin of humans. It is a Gram-positive, spherically shaped bacterium.[5] Staph infections can range from minor skin problems to life-threatening illness. *S. aureus* can cause a range of illnesses, from minor skin infections such as pimples, impetigo, boils, cellulitis, folliculitis, carbuncles, scalded skin syndrome, and abscesses to life-threatening diseases such as pneumonia, meningitis, osteomyelitis, endocarditis, toxic shock syndrome, and sepsis.[6] *S. aureus* is known for its alpha-toxin, which is a primary cytotoxic chemical and the first bacterial exotoxin recognized as pore-forming. *S. aureus* is a bacterium that causes staphylococcal food poisoning, a form of gastroenteritis with rapid onset of symptoms. Staph bacteria are one of the most common causes of food poisoning. The bacteria multiply in food and produce toxins.[7,8] Antibiotics are not useful in treating this illness because the toxin is not affected by antibiotics. *S. aureus* is a common cause of foodborne illness. *S. aureus* has a high level of antibiotic resistance and is a common cause of infections in hospitals and the community. Methicillin-resistant *S. aureus* (MRSA) is a type of staph infection that is difficult to treat because of resistance to some antibiotics.[9–11] The rising prevalence of community-acquired methicillin-resistant *S. aureus* (CA-MRSA), combined with the important severity of *S. aureus* infections in general, has resulted in the frequent use of anti-staphylococcal antibiotics, leading to increasing resistance rates.[9–11] Antibiotic-resistant *S. aureus* continues to be a major health concern, necessitating the development of novel therapeutic strategies.[12] *Escherichia coli* (*E. coli*) is a Gram-negative, facultative anaerobic, rod-shaped bacterium that is commonly found in the lower intestine of warm-blooded organisms. Most of the *E. coli* strains are harmless, but some can cause serious food poisoning.[13–16] *E. coli* infection can cause usually abdominal cramps, diarrhoea, and vomiting. If untreated, it may lead to complications such as severe dehydration, anaemia, mental changes such as confusion, kidney failure known as haemolytic uremic syndrome, and even death.[17] Certain strains release toxins that damage the lining of the small intestine. These toxins are known as Shiga toxins and the strains of *E. coli* that produce them are sometimes called STEC, which stands for "Shiga toxin-producing *E. coli*". Shiga toxin-producing *E. coli* (STEC) is a type of *E. coli* that can cause severe foodborne diseases.[13] Coliform bacteria include a large group of many types of bacteria that occur throughout the environment. They are common in soil and surface water and may even occur on your skin. To determine the appropriate antibiotics for treating an infection, the Kirby–Bauer test,[18] also known as the disk-diffusion method,[19] is commonly used. This technique measures bacterial growth inhibition under controlled conditions. The test organism is evenly and aseptically seeded onto a culture media, such as nutrient agar, and filter paper discs impregnated with a specific antibiotic at a given concentration are placed on the medium. The bacterium will proliferate on the agar plate if the antibacterial agent does not inhibit its growth. If the organism is susceptible, there will be no growth around the antibiotic-containing disc. As a result, a "zone of inhibition" can be seen and measured to determine an organism's susceptibility to an antibiotic.[18,20] The organism can be categorised as resistant (*R*), intermediate (*I*), or susceptible (*S*) based on the criteria.

The antimicrobial materials can be classified into two major categories based on their chemical composition: organic[21] and inorganic.[22] Organic materials include natural compounds derived from animal, plant, or microbial sources, such as plant extracts, essential oils, small antimicrobial peptides of animal origin and various groups of plant compounds (triterpenoids; alkaloids; phenols; flavonoids) with antimicrobial and antiviral activity. Organic antibacterial compounds often exhibit less stability, particularly under high temperature and pressure conditions, compared to their inorganic counterparts.[23] Recently, inorganic materials such as metals and metal oxides have garnered increased attention due to their resilience under challenging processing conditions and their broad acceptance as safe for both humans and animals. Inorganic nanomaterials are widely used in the treatment of tumours and bacterial infections due to their low toxicity, small size, good biocompatibility, easy modification, and large surface energy. The emergence of inorganic nanomaterials provides a new opportunity for the prevention and treatment of bacterial infection. Silver,[24–27] gold,[28–30] zinc,[31–35] copper,[36,37] and iron[38–40] nanoparticle types have shown tremendous potential as bactericidal and fungicidal elements, demonstrating their potential as efficient antibiotic reagents in wound care and related medical issues. The small size of the nanoparticles is very suitable for carrying out antimicrobial biological operations.[41] Inorganic materials include nanoparticles and composite films made of gold, silver, copper, zinc oxide, titanium oxide, magnesium oxide, and iron oxide. These materials have proven antimicrobial mechanisms and bio/cyto-compatibility. Inorganic antimicrobial materials can be photo-catalytic antimicrobial materials (activated by light), and nanomaterials that can directly lead to bacterial elimination or death (direct antimicrobial nanomaterials).

Among these, zinc oxide quantum dots (QDs) stand out due to their easy preparation process, green synthesis, cost-effectiveness, and safety for humans and animals. zinc oxide quantum dots (ZnO-QDs) have gained scientific attention due to their excellent antibacterial, antifungal, wound-healing, UV filtering, and semiconducting capabilities.[42–44] They also have high catalytic and photochemical activity, making them applicable in various fields. Several processes can be used to synthesize zinc oxide quantum dots, including wet chemical, chemical microemulsion, hydrothermal, vapour phase, solvothermal, microwave-assisted combustion, chemical, direct precipitation, and sono-chemical or green synthesis methods.[44–48] This study represented the addition of zinc oxide quantum dots in the bis MPA polyester-64-hydroxyl dendrimer with five different numbers of surface functional groups functionalized. The resulting ZnO-QDs @ bis MPA polyester-64-hydroxyl dendrimer nanostructures exhibited unique characteristics and tuneable chemical and physical properties. The approach used to create these ZnO-QDs @ bis MPA polyester-64-hydroxyl dendrimer nanostructures was cost-effective, easy, and environmentally friendly. Additionally, the antibacterial properties of the generated zinc oxide quantum dots were tested against pathogenic microorganisms. These ZnO-QDs @ bis MPA polyester-64-hydroxyl dendrimer nanostructures play a significant role in the development of sustainable products. The use of ZnO in dendrimers has shown promising results in terms of their antibacterial properties and potential applications in sustainable materials. This work demonstrates the potential of using a simple and cost-effective approach to create ZnO-QDs @ bis MPA polyester-64-hydroxyl dendrimer nanostructures. Further research is needed to fully understand the potential applications of these nanostructures in scientific fields.

Results and discussion

The bis MPA polyester-64-hydroxyl dendrimer was functionalized with zinc oxide quantum dots that had five different selective levels of surface functionalization: 1, 5, 10, 20, and 40. The functionalization with 80 hydroxyl surface groups gives negative results *i.e.*, only starting materials shows UV spectra due to unavailability of surface groups on the dendritic structure. Five distinct ZnO-QDs @ bis MPA polyester-64-hydroxyl dendrimer nanostructures were identified during the process, each exhibiting unique properties. The ZnO-QD functionalization influenced the optical, electrical, chemical, physical and antibacterial properties of the ZnO-QDs @ bis MPA polyester-64-hydroxyl dendrimer nanostructures. The functionalization compared the properties of the ZnO-QDs @ bis MPA polyester-64-hydroxyl dendrimer nanostructures with different degrees of functionalization. Here the zinc oxide quantum dots were successfully synthesized using sonochemistry and subsequently characterized using a variety of techniques.[44–48] These included UV-vis-NIR spectroscopy, ATR-FTIR spectroscopy, Raman spectroscopy, DLS and XRD spectroscopy. The data obtained from these characterization studies were found to be in close agreement with the data presented in available research databases.

The synthesized zinc oxide quantum dots have been used for ZnO-QDs @ bis MPA polyester-64-hydroxyl dendrimer nanostructure formulation. The hydroxyl groups eliminated by zinc oxide quantum dots form novel ZnO-QDs @ bis MPA polyester-64-hydroxyl dendrimer nanostructures. Sodium borohydride is a mild reducing agent that can convert aldehydes and ketones into alcohols while selectively reducing esters due to its delayed reaction. The added metal provides stability and speeds up the reaction when employing sodium borohydride solutions for large-scale ester reduction at 25 °C.[49] In addition to giving zinc oxide quantum dots stability, sodium borohydride can reduce ester to C–H bonds. This synthetic process produced a novel structure with unique physicochemical characteristics. The ester to C–H bond of the bis MPA polyester-64-hydroxyl dendrimer was reduced by sodium borohydride in the ZnO-QDs @ dendrimer and provides stability to zinc oxide quantum dots. All synthesized nanostructures have different characteristic properties compared to those of the original bis MPA polyester-64-hydroxyl dendrimer as represented below.

Characterization techniques for ZnO-QDs @ bis MPA polyester-64-hydroxyl dendrimer nanostructures

These five novel ZnO-QDs @ bis MPA polyester-64-hydroxyl dendrimer nanostructures are achieved after functionalization of the bis MPA polyester-64-hydroxyl dendrimer with zinc oxide quantum dots. The bis MPA polyester-64-hydroxyl dendrimer acts as a stabilising agent for the zinc oxide quantum dots, preventing them from aggregating or precipitating. The stability of these zinc oxide quantum dots is ensured by the functionalization of a bis MPA polyester-64-hydroxyl dendrimer, which acts as a protective shell, preventing degradation and maintaining the integrity of the zinc oxide quantum dots. The ZnO-QDs @ bis MPA polyester-64-hydroxyl dendrimer nanostructures have unique chemical and physical characteristics, such as solubility, crystallinity, molecular vibration, and morphology. The ZnO-QDs @ bis MPA polyester-64-hydroxyl dendrimer nanostructures exhibit different optical properties than the pure bis MPA polyester-64-hydroxyl dendrimer and zinc oxide quantum dots, as evidenced by the ultraviolet-visible spectroscopy analysis. The bis MPA polyester-64-hydroxyl dendrimer G4-R(ZnO-QDs)$_n$ were dispersed in water at a concentration of 0.2% w/v before the ultraviolet-visible-NIR (UV-vis-NIR) measurement was carried out using the sample. The absorbance max (λ_{max}) was observed at room temperature spanning 200–1200 nm. A cuvette with a 1 cm path length was used to scan the material. The starting material bis MPA polyester-64-hydroxyl dendrimer and zinc oxide quantum dots have maximum intensity absorption wavelengths (λ_{max}) of 351 nm and 340 nm, respectively. Nanostructure G4-R(ZnO-QDs)$_1$, G4-R(ZnO-QDs)$_5$, G4-R(ZnO-QDs)$_{10}$, G4-R(ZnO-QDs)$_{20}$, and G4-R(ZnO-QDs)$_{40}$ have maximum intensity absorption wavelengths of 301 nm, 301 nm, 303 nm, 305 nm, and 306 nm; 347 nm, respectively. Fig. 1 depicts the UV-vis-NIR absorption spectra of the bis MPA polyester-64-hydroxyl dendrimer nano-structure using UV-vis-NIR spectroscopy The absorption spectra of the ZnO-QDs @ bis MPA polyester-64-hydroxyl dendrimer
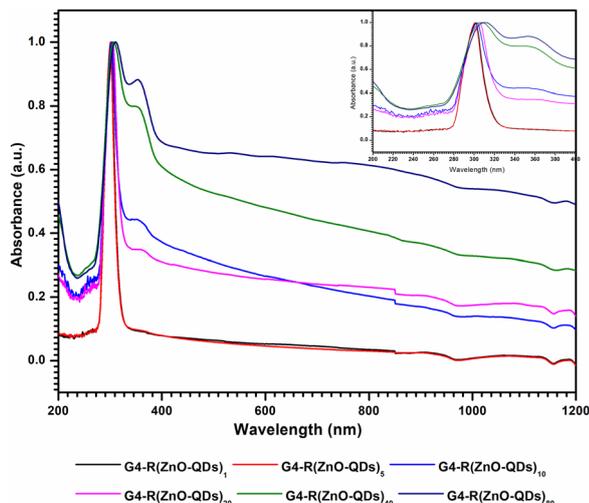
Fig. 1 UV-vis-NIR absorption spectrum of ZnO-QDs @ bis MPA poly-ester-64-hydroxyl dendrimer nanostructures.

nanostructures show a hypsochromic shift, which means that they absorb light at shorter wavelengths and a shift of the band to higher energy compared to that of the pure components. This blue shift in the spectrum is indicative of each ZnO-QDs @ bis MPA polyester-64-hydroxyl dendrimer nanostructure possessing distinct optical properties, further emphasizing their uniqueness. This indicates that the interaction and chemical bonding between the bis MPA polyester-64-hydroxyl dendrimer and the zinc oxide quantum dots alter the electronic structure of the ZnO-QDs @ bis MPA polyester-64-hydroxyl dendrimer nanostructures. One of the most exciting features of these ZnO-QDs @ bis MPA polyester-64-hydroxyl dendrimer nanostructures is their solubility. Unlike the water-insoluble bis MPA polyester-64-hydroxyl dendrimer and zinc oxide quantum dots, the new five ZnO-QDs @ bis MPA polyester-64-hydroxyl dendrimer nanostructures are water-soluble due to their hydrophilic nature. This property opens up a plethora of potential applications in various fields where water solubility is a prerequisite.

The infrared spectrum of ZnO-QDs @ bis MPA polyester-64-hydroxyl dendrimer nanostructures was analysed by a powerful technique called attenuated total reflectance-Fourier transform infrared spectroscopy (ATR-FTIR). This technique uses a beam of infrared light that reflects off the surface of the material and measures the amount of absorption. The novel ZnO-QDs @ bis MPA polyester-64-hydroxyl dendrimer nanostructures under investigation have been found to possess unique vibrational frequencies that can absorb two primary types of infrared radiation. The ATR-FTIR measurements were conducted over a spectral range of 1200 to 2000 cm^{-1}. The results revealed that the ZnO-QDs @ bis MPA polyester-64-hydroxyl dendrimer nanostructures displayed a prominent peak at 1724.61 cm^{-1}. This peak is indicative of the C=O stretching vibration present of an α,β-unsaturated ester group functional group in the bis MPA polyester-64-hydroxyl dendrimer. Interestingly, as the concentration of zinc oxide quantum dots on the surface

functional groups increased, a clear decrease in the intensity of the absorbed vibrational frequency band of the α,β-unsaturated ester group at 1724.613 cm^{-1} was observed. This decrease was accompanied by a corresponding increase in the intensity of the absorbed vibrational frequency band at 1550 cm^{-1}. The ATR-FTIR data thus show that the surface hydroxyl functional groups were eliminated upon the addition of zinc oxide quantum dots to the surface functional groups. This elimination resulted in an increase in the intensity of the absorbed vibrational frequency band at 1550 cm^{-1}. These findings could have significant implications for the development of new nanostructures with tailored infrared absorption properties. Fig. 2 depicts FTIR spectra of the ZnO-QDs @ bis MPA polyester-64-hydroxyl dendrimer nanostructures using ATR-FTIR spectroscopy.

Fig. 3 depicts the Raman spectra of ZnO-QDs @ bis MPA polyester-64-hydroxyl dendrimer nanostructures in the 100–3200 cm^{-1} range. The Raman spectra exhibit unique a bis MPA polyester-64-hydroxyl dendrimer fingerprint. The Raman band at 1458 cm^{-1} was indicative of (CH$_2$) and (CH$_3$) bending asymmetric vibrations, (C–O–C) stretching vibration at 858 cm^{-1}, (C=O) stretching vibrations at 1724 cm^{-1}, and lattice vibrations in crystals at 119 cm^{-1}. Raman shifts at 2883 cm^{-1}, 2945 cm^{-1}, and 2976 cm^{-1} were responses to the (CH) stretching vibrations. Raman shifts at 912 cm^{-1} and 1008 cm^{-1} were responses to the (CC) alicyclic, aliphatic chain stretching vibration. Raman shifts at 646 cm^{-1}, 750 cm^{-1}, 912 cm^{-1}, 1008 cm^{-1}, 1054 cm^{-1}, 1143 cm^{-1}, and 1281 cm^{-1} were responses to the (CC) alicyclic, aliphatic chain stretching vibrations. The following minor Raman bands were observed in the Raman spectra of G4-R(ZnO-QDs)$_1$: the Raman shift at 664 cm^{-1} was a response to the stretching vibrations of the (CC) alicyclic, aliphatic chain. The following minor Raman bands were observed in the Raman spectra of G4-R(ZnO-QDs)$_5$: the Raman shift at 664 cm^{-1} was a response to the stretching vibrations of the (CC) alicyclic, aliphatic chain. The Raman band at 331 cm^{-1} indicated bending vibration of (CC) aliphatic chains, whereas the Raman band at 128 cm^{-1} indicated crystal lattice vibrations.
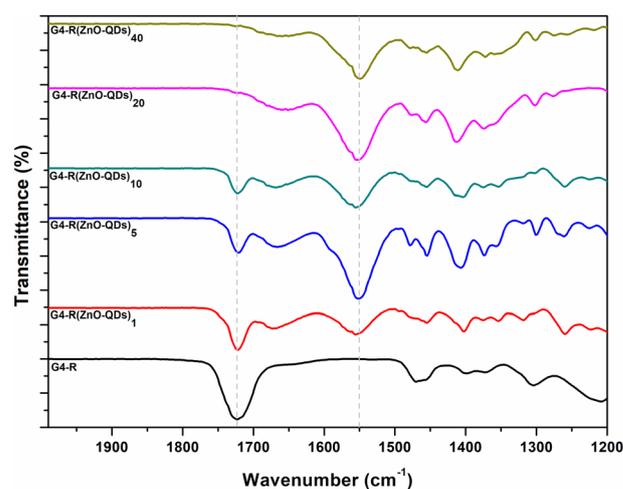

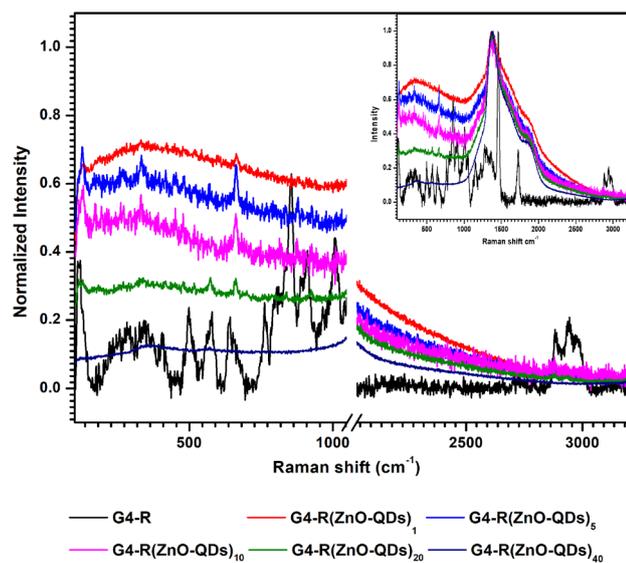Fig. 2 FTIR spectra of the ZnO-QDs @ bis MPA polyester-64-hydroxyl dendrimer nanostructures.

Fig. 3 Raman spectra of bis MPA polyester-64-hydroxyl dendrimer and ZnO-QDs @ bis MPA polyester-64-hydroxyl dendrimer nanostructures (1050–2050 cm^{-1} shows peaks due to the glass slide, that is eliminated in the enlarged graph).

The following minor Raman bands are observed in the Raman spectra of G4-R(ZnO-QDs)$_{10}$: the crystal lattice vibration frequency was 128 cm^{-1}. Raman shifts at 664 cm^{-1} were responses to stretching vibrations of the (CC) alicyclic, aliphatic chain. The Raman band at 331 cm^{-1} was indicative of the bending vibration of (CC) aliphatic chains. The following minor Raman bands are observed in the Raman spectra of G4-R(ZnO-QDs)$_{20}$: Raman shifts at 661 cm^{-1} and 924 cm^{-1} were responses to stretching vibrations of the (CC) alicyclic, aliphatic chain. The crystal lattice vibration frequency was 128 cm^{-1}. The Raman spectra of G4-R(ZnO-QDs)$_{40}$ showed the absence of a recognisable Raman band. The structural vibration patterns of the ZnO-QDs @ bis MPA polyester-64-hydroxyl dendrimer nanostructures, particularly differ from those of the pure bis MPA polyester-64-hydroxyl dendrimer and zinc oxide quantum dots analysed by using the Raman spectra. The Raman spectra reveal unexpected and startling responses, which is another intriguing aspect of these ZnO-QDs @ bis MPA polyester-64-hydroxyl dendrimer nanostructures. According to the Raman spectra, the ZnO-QDs @ bis MPA polyester-64-hydroxyl dendrimer nanostructures have a complex structure that involves chemical bonding, intra-molecular interactions and physical interactions between the bis MPA polyester-64-hydroxyl dendrimer and the zinc oxide quantum dots. The crystalline nature of both the bis MPA polyester-64-hydroxyl dendrimer and zinc oxide quantum dots was expected. However, the Raman spectra of these ZnO-QDs @ bis MPA polyester-64-hydroxyl dendrimer nanostructures revealed an unanticipated response identified as amorphous nanostructures, found just because of surface electronegativity and intra-molecular interactions. Each of the five ZnO-QDs @ bis MPA polyester-64-hydroxyl dendrimer nanostructures exhibited a unique molecular vibration spectrum, further highlighting their individuality. In Fig. 3, Raman

spectra of ZnO-QDs @ bis MPA polyester-64-hydroxyl dendrimer nanostructures at 1050–2050 cm^{-1} were eliminated in the enlarged graph. It shows peaks due to the glass slide.

The size determination of all five nanostructures was executed by two different techniques: dynamic light scattering (DLS) and atomic force microscopy (AFM). DLS is an essential technique for nanoparticle size analysis that has been employed extensively for decades. The size and size distribution of the particles in the colloids were determined (Malvern Instruments) using a Nano ZS Zetasizer system. The following measurement parameters were used: a He–Ne laser with a wavelength of 633 nm, a fixed scattering angle of 173°, a measurement temperature of 25 °C, a medium viscosity of 0.8872 mPas, a medium refractive index of 1.330, and a material refractive index of 1.33. Before DLS analysis, the colloid was filtered through a Millipore syringe filter with a 0.2 μm polyvinylidene fluoride (PVDF) membrane. Three measurements were made with the material placed in a quartz microcuvette, and the average result was recorded. The size distribution of dendrimer nanostructures was found to be in the nanometre range. The bis MPA polyester-64-hydroxyl dendrimer G4-R(ZnO-QDs)$_n$ nanostructures were suspended in distilled water. The DLS size shows the hydrodynamic diameter of the particles as measured by DLS, which takes into account not only the size of the particle itself but also any surrounding layers of solvent or other molecules that may affect its movement in solution. The PDI shows the polydispersity index, which is a measure of the distribution of particle sizes in a sample. A lower PDI value indicates a more uniform distribution of particle sizes. The PDI is a measure of the distribution of molecular mass in a ZnO-QDs @ bis MPA polyester-64-hydroxyl dendrimer nanostructure sample. PDI values close to 0 indicate a very uniform sample, while larger values indicate a broader distribution of sizes.

Atomic force microscopy (AFM) is a powerful technique used for visualizing and characterizing nanoscale structures with high resolution. Nanostructure size analysis and 3D imaging were carried out by using a Bruker Multimode 8 AFM probe microscope. A 0.1% bis MPA polyester-64-hydroxyl dendrimer G4-R(ZnO-QDs)$_n$ nanostructure solution was prepared in water. The bis MPA polyester-64-hydroxyl dendrimer G4-R(ZnO-QDs)$_n$ nanostructures were dispersed in the solvent for a stable colloidal suspension. These samples were used for imaging the dendrimer nanostructures. A mica plate was chosen as the substrate for imaging. Prior to sample loading, the mica surface was meticulously cleaned using cello tape to remove any contaminants. The drop-casting method was employed to load the sample onto the mica plate. A droplet of the solution was placed on the mica surface and allowed to dry. After overnight drying, the sample was gently dried with nitrogen gas to ensure complete removal of any remaining solvent. The prepared samples were now ready for imaging. All bis MPA polyester-64-hydroxyl dendrimer G4-R(ZnO-QDs)$_n$ nanostructures were scanned at a scan size of 1.0 μm × 1.0 μm. The scan rate was 1 Hz per scan line using AFM. These parameters were chosen to achieve a balance between imaging speed and resolution. Smaller scan sizes allow for higher resolution but may increase imaging time. However, raw AFM images often contain artifacts

due to the imaging process. To improve image quality, a line-wise zero order flattening was applied. This step removes any systematic height variations introduced during scanning. The resulting flattened image provides a more accurate representation of the sample's topography. The particle size is determined by analysing cross-sectional line profiles. The cross-sectional data can be used to determine characteristics such as the nanostructure size and the surface roughness through the analysis of various cross-sectional profiles.[50] AFM provides valuable insights into bis MPA polyester-64-hydroxyl dendrimer G4-R(ZnO-QDs)$_n$ nanostructure morphology, allowing the visualization of 3D structures and accurate measurement of particle sizes. The combination of sample preparation, precise scan parameters, and thoughtful image analysis ensures reliable results in nanostructure characterization.

On the other hand, Atomic Force Microscopy (AFM) was another technique used to measure the physical size of nanostructures. Additionally, differences in sample preparation and measurement conditions can also affect the results obtained using these two techniques. The nano-sized diameter of the ZnO-QDs @ bis MPA polyester-64-hydroxyl dendrimer nanostructures was determined using AFM data. Fig. 4 depicts the Dynamic Light Scattering (DLS) spectra of the synthesized ZnO-QDs @ bis MPA polyester-64-hydroxyl dendrimer nanostructures. Fig. 5 depicts the AFM images of the synthesized ZnO-QDs @ bis MPA polyester-64-hydroxyl dendrimer nanostructures in two dimensions, three-dimensions and the cross section profile G4-R(ZnO-QDs)$_1$ has a DLS size of 90.30 nm with a PDI of 0.08, and an AFM size of 16 nm $\pm$ 0.56 nm. This means that when measured using DLS, the average hydrodynamic diameter of the particles in G4-R(ZnO-QDs)$_1$ was found to be 90.30 nm, and the distribution of particle sizes was relatively uniform, as indicated by the low PDI value. When measured using AFM, the size of the particles was found to be 16 nm $\pm$ 0.56 nm with a line roughness of 1.08 nm. G4-R(ZnO-QDs)$_5$ has a DLS size of 50.75 nm with a PDI of 0.05, and an AFM size of 8 nm $\pm$ 0.02 nm. This means that when measured using DLS, the average hydrodynamic diameter of the particles in nanomaterial G4-R(ZnO-QDs)$_5$ was found to be 50.75 nm, and the distribution of particle sizes was relatively uniform, as indicated by the low PDI value. When measured using AFM, the size of the

A: G$_4$ bis MPA polyester; B:G$_4$-R(ZnO$_1$); C:G$_4$-R(ZnO$_5$); D:G$_4$-R(ZnO$_{10}$); E: G$_4$-R(ZnO$_{20}$), F: G4-R(ZnO$_{40}$)
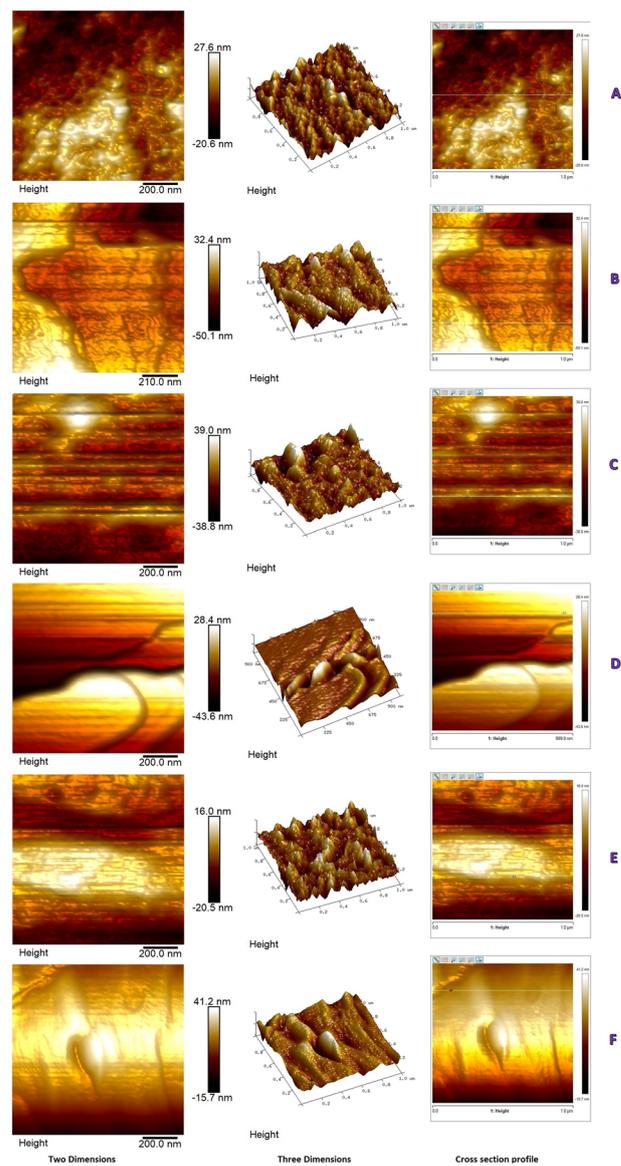
Fig. 5 Atomic Force Microscopy (AFM) 2D images, 3D images and cross section of (A) the bis MPA polyester-64-hydroxyl dendrimer and (B–F) ZnO-QDs @ bis MPA polyester-64-hydroxyl dendrimer nanostructures.

A: ZnO QDs; B:G$_4$-R(ZnO$_1$); C:G$_4$-R(ZnO$_5$); D:G$_4$-R(ZnO$_{10}$); E: G$_4$-R(ZnO$_{20}$), F: G4-R(ZnO$_{40}$)
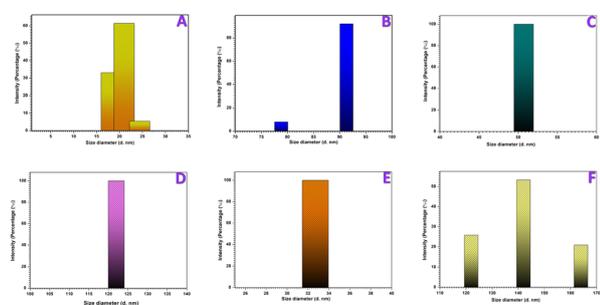
Fig. 4 Particle size distribution by intensity (A) zinc oxide quantum dots and (B–F) ZnO-QDs @ bis MPA polyester-64-hydroxyl dendrimer nanostructures.

particles was found to be 8 nm $\pm$ 0.02 nm with a line roughness of 2.13 nm. G4-R(ZnO-QDs)$_{10}$ has a DLS size of 122.4 nm with a PDI of 0.08, and an AFM size of 12.04 nm $\pm$ 0.004 nm. This means that when measured using DLS, the average hydrodynamic diameter of the particles in nanomaterial G4-R(ZnO-QDs)$_{10}$ was found to be 122.4 nm, and the distribution of particle sizes was relatively uniform, as indicated by the low PDI value. When measured using AFM, the size of the particles was found to be 12.04 nm $\pm$ 0.004 nm with a line roughness of 0.02 nm. G4-R(ZnO-QDs)$_{20}$ has a DLS size of 32.67 nm with a PDI of 0.03, and an AFM size of 16 nm $\pm$ 0.05 nm. This means that when measured using DLS, the average hydrodynamic diameter of the particles in nanomaterial G4-R(ZnO-QDs)$_{20}$ was found to
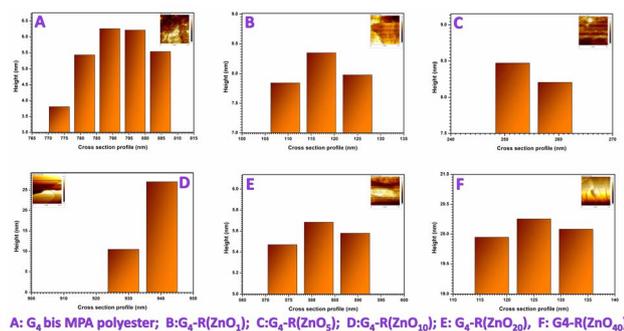
Fig. 6 Atomic Force Microscopy (AFM) cross section profile of (A) the bis MPA polyester-64-hydroxyl dendrimer and (B–F) ZnO-QDs @ bis MPA polyester-64-hydroxyl dendrimer nanostructures.

be 32.67 nm, and the distribution of particle sizes was relatively uniform, as indicated by the low PDI value. When measured using AFM, the size of the particles was found to be 16 nm $\pm$ 0.05 nm with a line roughness of 0.33 nm. G4-R(ZnO-QDs)$_{40}$ has a DLS size of 141.5 nm with a PDI of 0.1, and an AFM size of 15.74 nm $\pm$ 0.80 nm. This means that when measured using DLS, the average hydrodynamic diameter of the particles in nanomaterial G4-R(ZnO-QDs)$_{40}$ was found to be 141.5 nm, and the distribution of particle sizes was relatively uniform, as indicated by the low PDI value. When measured using AFM, the size of the particles was found to be 15.74 nm $\pm$ 0.80 nm with a line roughness of 1.39 nm. The morphology of the nanomaterials was investigated by atomic force microscopy (AFM), which showed that they have a spherical shape with a non-uniform size distribution. The three-dimensional ZnO-QDs @ bis MPA polyester-64-hydroxyl dendrimer nanostructure distribution was observed in the nanometre scale size range of less than 100 nm. The AFM analysis was performed, and the analysis indicated that the smallest particle had a diameter of 7.9 nm in ZnO-QDs @ bis MPA polyester-64-hydroxyl dendrimer nanostructures. The ZnO-QDs @ bis MPA polyester-64-hydroxyl dendrimer nanostructures were synthesized with less than 20 nm size, which enhances the surface area. Fig. 6 depicts the AFM cross section profile and histogram data of the synthesized ZnO-QDs @ bis MPA polyester-64-hydroxyl dendrimer nanostructures.

The size of the ZnO-QDs @ bis MPA polyester-64-hydroxyl dendrimer nanostructures affects their surface area, which is an important parameter for their antibacterial, catalytic, adsorptive, and optical properties. The AFM analysis also revealed that

the surface roughness of the ZnO-QDs @ bis MPA polyester-64-hydroxyl dendrimer nanostructures decreases as the zinc oxide quantum dot functionalization of surface functional groups increases in the bis MPA polyester-64-hydroxyl dendrimer. Interestingly, as zinc oxide quantum dot functionalization increased, the surface roughness decreased.

Further AFM analysis determined that the surface roughness of bis MPA polyester-64-hydroxyl dendrimer G4-R(ZnO-QDs)$_n$ nanostructures is included in Table 1, where R_q = standard deviation of the Z values within the surface area, R_a = arithmetic average of the absolute values of the surface height deviations measured from the mean plane within the surface area, and R_{max} = roughness R_{max} plane within the surface area.

This implies that the zinc oxide quantum dots smooth out the surface of the bis MPA polyester-64-hydroxyl dendrimer, creating more homogeneous and uniform ZnO-QDs @ bis MPA polyester-64-hydroxyl dendrimer nanostructures. This smaller size significantly enhances their surface area, making them more efficient in various applications. This topological distribution provides valuable insights into the behaviours of these novel ZnO-QDs @ bis MPA polyester-64-hydroxyl dendrimer nanostructures.

Mechanism of action for antibacterial agents

Attention has been attracted worldwide by zinc oxide nanoparticles (ZnO-NPs) due to their antibacterial properties. The size range between hundreds of nano-meters and tens of micrometres is home to various microorganisms. The novel nanostructures are making efforts to improve the antibacterial activities of zinc oxide quantum dots by functionalization with surface functional groups. The increased specific surface area and higher surface reactivity of ZnO-QDs @ bis MPA polyester-64-hydroxyl dendrimer nanostructures and their reduced particle size provide desirable antibacterial capabilities. Zinc oxide quantum dots are a less hazardous substance with photo-oxidising and photo-catalytic effects on chemical and biological species. Forming a nanostructure reduces electron/hole recombination, increases the surface area to volume ratio, and also improves the stability towards dissolution and corrosion. The release of antimicrobial ions, electrostatic interaction, and reactive oxygen species (ROS)[51] generations are the crucial antibacterial activity mechanism. With a focus on the production of reactive oxygen species (ROS) such as hydrogen peroxide (H_2O_2), hydroxyl radicals, and O_2^{2-}, particular attention was placed on bactericidal and bacteriostatic processes (peroxide). Several mechanisms, such as cell wall destruction by

Table 1 Surface roughness of bis MPA polyester-64-hydroxyl dendrimer G4-R(ZnO-QDs)$_n$ nanostructures

	R_q	R_a	R_{max}
Bis MPA polyester-64-hydroxyl dendrimer	1.79 nm	1.41 nm	10.4 nm
G4-R(ZnO-QDs)$_1$ dendrimer nanostructures	1.96 nm	1.59 nm	8.71 nm
G4-R(ZnO-QDs)$_5$ dendrimer nanostructures	1.59 nm	1.24 nm	7.20 nm
G4-R(ZnO-QDs)$_{10}$ dendrimer nanostructures	0.882 nm	0.706 nm	5.41 nm
G4-R(ZnO-QDs)$_{20}$ dendrimer nanostructures	0.945 nm	0.752 nm	5.15 nm
G4-R(ZnO-QDs)$_{40}$ dendrimer nanostructures	0.459 nm	0.376 nm	2.39 nm

nanoparticle interactions, increased membrane permeability, internalisation of QDs brought on by the loss of proton motive force, and uptake of hazardous dissolved zinc ions, have been greatly influenced by ROS. The ZnO-QDs @ bis MPA polyester-64-hydroxyl dendrimer nanostructures are a new class of nanoscale particle size-range antibacterial active nanostructures. They have unique physicochemical characteristics that can affect biological and toxicological responses in microorganisms. These have resulted in mitochondrial weakening, intracellular leakage, and release of oxidative stress-related gene expression, which ultimately caused cell growth inhibition and cell death. In some instances, surface flaws on the abrasive surface defects of ZnO can be blamed for increased antibacterial activity.[51] The bis MPA polyester-64-hydroxyl dendrimer must be a biodegradable,[52] biocompatible carrier. The bis MPA polyester-64-hydroxyl dendrimer was found to be resistant toward both bacteria. When nanostructures were functionalised with different numbers of zinc oxide quantum dots they becomes active toward bacteria. The bis MPA polyester-64-hydroxyl dendrimers were functionalised to improve the antibacterial activities of zinc oxide quantum dots by forming a new ZnO-QDs @ bis MPA polyester-64-hydroxyl dendrimer nanostructure. The bis MPA polyester-64-hydroxyl dendrimer can control the morphology and size of the nanostructure, and optimizing different conditions also enhanced the antibacterial activity.[51]

Antibacterial activity of ZnO-QDs @ bis MPA polyester-64-hydroxyl dendrimer nanostructures

The bis MPA polyester-64-hydroxyl dendrimer is resistant toward both bacterial strains and bacterial species. Due to ether functionality modified zinc oxide quantum dots carrying electronegative oxygen species, compounds were tested for their antibacterial activity against Gram-positive (*S. aureus*) and Gram-negative (*E. coli*) human pathogenic bacterial strains. The results of an experiment where different nanostructures were tested against *S. aureus* and *E. coli* bacteria shown by disk diffusion technique. Fig. 7 depicts the antimicrobial activity of the ZnO-QDs @ bis MPA polyester-64-hydroxyl dendrimer nano-
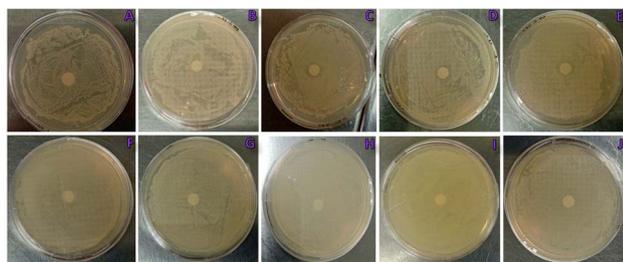

Fig. 7 Antimicrobial activity of the dendrimer nano-structure in terms of the zone of inhibition (mm). Images of agar plates showing the zone of inhibition of (A): G4-R(ZnO-QDs)$_1$(*S. aureus*); (B):G4-R(ZnO-QDs)$_5$ (*S. aureus*); (C): G4-R(ZnO-QDs)$_{10}$ (*S. aureus*); (D): G4-R(ZnO-QDs)$_{20}$ (*S. aureus*); (E): G4-R(ZnO-QDs)$_{40}$ (*S. aureus*); (F): G4-R(ZnO-QDs)$_1$ (*E. coli*); (G): G4-R(ZnO-QDs)$_5$ (*E. coli*); (H): G4-R(ZnO-QDs)$_{10}$ (*E. coli*); (I): G4-R(ZnO-QDs)$_{20}$ (*E. coli*); (J): G4-R(ZnO-QDs)$_{40}$ (*E. coli*).

structure. The nanostructures were tested at a dose of 50 μg μl^{-1}. The zone diameter is the area around the nanostructure loaded disk where bacterial growth is inhibited. A larger zone diameter indicates that the bacteria are more susceptible to the nanostructures, while a smaller zone diameter or no zone at all indicates that the bacteria are resistant to the nanostructures. The zone diameter in *S. aureus* for nanostructures G4-R(ZnO-QDs)$_1$ and G4-R(ZnO-QDs)$_5$ was 0 mm, indicating no inhibition of bacterial growth. Nanostructures G4-R(ZnO-QDs)$_{10}$, G4-R(ZnO-QDs)$_{20}$ and G4-FR(ZnO-QDs)$_{40}$ showed inhibition of bacterial growth in *S. aureus* with zone diameters of 7 mm, 8 mm, and 10 mm, respectively. None of the nanostructures showed any inhibition of bacterial growth in *E. coli*, with all zone diameters being 0 mm. *S. aureus* is susceptible to nanostructures G4-R(ZnO-QDs)$_{10}$, G4-R(ZnO-QDs)$_{20}$ and G4-R(ZnO-QDs)$_{40}$ at a dose of 50 μg μl^{-1}, while *E. coli* is resistant to all five nanostructures tested at this dose. Compared to standard ZnO NPs, this is relevant to bacterial species in terms of inhibitory and resistant nature. The ZnO-QDs @ bis MPA polyester-64-hydroxyl dendrimer nanostructure antibacterial assay results are similar to those of the ZnO NP antimicrobial properties for Gram-positive and Gram-negative bacterial species. Thus, the ability of the ZnO-QDs @ bis MPA polyester-64-hydroxyl dendrimer nanostructures to cross the outer membrane or cell wall in Gram-positive bacteria is dependent on the introduction of oxygen in the cyclic bond with the bis MPA polyester-64-hydroxyl dendrimer, and ZnO-QDs @ bis MPA polyester-64-hydroxyl dendrimer nanostructures provided higher surface area which increases the ability to irritate the cell membranes or inhibits of bacterial growth. The bis MPA polyester-64-hydroxyl dendrimer must enhance stability of zinc oxide quantum dots, permissibility, surface area, and nano-size of novel ZnO-QDs @ bis MPA polyester-64-hydroxyl dendrimer nanostructures and antibacterial activity.

Determination of the inhibitory concentration of 50% (IC50) and 90% (IC90) of the microorganisms

The confirmed parameters ensured that the conventional methodology was observed to determine inhibitory doses of 50% (IC$_{50}$) and 90% (IC$_{90}$) of the antibacterial activity. Since the values of R^2 are greater than 0.95 for *S. aureus* in the Kirby Bauer Disk Diffusion experiment, the percentage inhibition with antimicrobial agent doses was observed to be linear. The straight-line equations are shown in Fig. 8. Building curves of correlation between percentage inhibition and concentration of the nanostructure was necessary to determine the IC$_{50}$ and IC$_{90}$. The inhibitory concentration percentage determined IC$_{50}$ and IC$_{90}$ values for different nanostructures. The IC$_{50}$ value is the concentration of a substance needed to inhibit the growth of 50% of the test organisms, while the IC$_{90}$ value is the concentration needed to inhibit the growth of 90% of the test organisms. Nanostructures G4-R(ZnO-QDs)$_1$ and G4-R(ZnO-QDs)$_5$ are resistant to both IC$_{50}$ and IC$_{90}$ values, while nanostructures G4-R(ZnO-QDs)$_{10}$, G4-R(ZnO-QDs)$_{20}$, and G4-R(ZnO-QDs)$_{40}$ have varying levels of sensitivity, with nanomaterial G4-R(ZnO-QDs)$_{40}$ being the most sensitive with an IC$_{50}$ value of 282.30 and
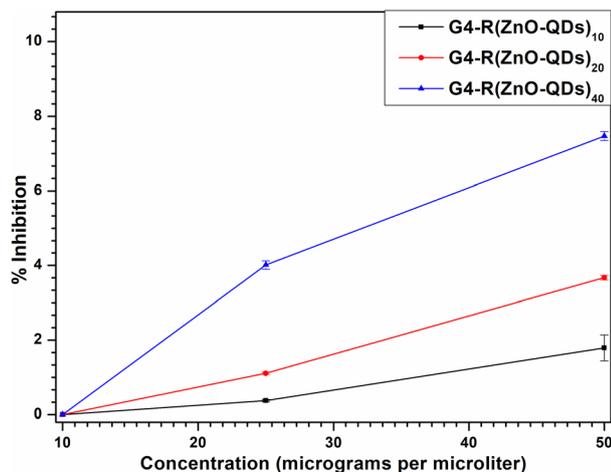
Fig. 8 Scatter diagram curves of the correlation between percentage inhibition and concentration of the nanostructure.

an IC_{90} value of 502.33. Nanostructure G4-R(ZnO-QDs)$_{10}$ has an IC_{50} value of 1099.56 and an IC_{90} value of 1969.13, while nanostructure G4-R(ZnO-QDs)$_{20}$ has an IC_{50} value of 549.38 and an IC_{90} value of 979.95. These curves are used to evaluate the method's validation parameters and determine the IC_{50} and IC_{90}.

In conclusion, this work has successfully synthesized five unique ZnO-QDs @ bis MPA polyester-64-hydroxyl dendrimer nanostructures with distinct properties and potential applications. The ZnO-QDs @ bis MPA polyester-64-hydroxyl dendrimer nanostructures have high-water solubility, a complex molecular vibration spectrum, antibacterial activity, and a spherical morphology with variable size and surface roughness. These features make them potential and promising candidates for various applications in science and technology.

Experimental

Materials required

Zinc oxide quantum dots (ZnO-QDs), hyper-branched bis-MPA polyester-64-hydroxyl – generation 4, sodium borohydride (NaBH$_4$), S. aureus (Staphylococcus aureus_ATCC 25923), E. coli (Escherichia coli _ATCC 25922), a 37 °C incubator, an autoclave, an analytical weight balance, a magnetic stirrer, magnetic stirring beads, a vortexer, sterile nichrome wire, a spreader, nutrient agar, Milli Q water, acetone, sterile 30 mm plates, Whatman filter paper, susceptibility disks, and a round bottom flask.

Methods

Synthesis of ZnO-QDs @ bis MPA polyester-64-hydroxyl dendrimer nanostructures: G4-R(ZnO-QDs)$_1$, G4-R(ZnO-QDs)$_5$, G4-R(ZnO-QDs)$_{10}$, G4-R(ZnO-QDs)$_{20}$, and G4-R(ZnO-QDs)$_{40}$. The in situ formation of zinc oxide quantum dots stabilized by the bis MPA polyester-64-hydroxyl dendrimer was carried out by adding zinc oxide quantum dots into bis MPA polyester-64-hydroxyl dendrimer solution and subsequent reduction with

NaBH$_4$. In a typical experiment, 100 mg of bis-MPA polyester-64-hydroxyl generation 4 (G4-R) was added to 5 ml of acetone; the mixture was stirred. One drop of distilled water was injected into the bis MPA polyester-64-hydroxyl dendrimer to dissolve the suspended particles (G4-R). Zinc oxide quantum dots (1.11 mg, 5.56 mg, 11.12 mg, 22.23 mg, and 44.46 mg) were individually added to 20 ml of a polymer solution. The reaction mixture was vigorously stirred for 18 h at room temperature. Subsequently, a fresh aqueous solution of NaBH$_4$ (33.08 mg in 20 ml) was added dropwise to the reaction mixture in an ice bath. The reaction was carried out for at least 3 h[53] The ice bath was removed to achieve room temperature. The reaction was monitored by using UV-vis-NIR spectroscopy. The reaction mixture was evaporated using a rotary evaporator. Hexane was used to wash the product three times, and after that, the solvent was evaporated using a rotary evaporator. As an outcome, a complex with surface functional groups of the bis MPA polyester-64-hydroxyl dendrimer (G4-R) is known as G4-R (ZnO-QDs)$_n$. The reduction reaction formed a complex G4-R(ZnO-QDs) using sodium borohydride. The %yield of the bis MPA polyester-64-hydroxyl dendrimer G4-R(ZnO-QDs)$_n$ nano-structure was found to be 94.2%, 92.8%, 95.0%, 90.6%, and 91.1% for G4-R(ZnO-QDs)$_1$, G4-R(ZnO-QDs)$_5$, G4-R(ZnO-QDs)$_{10}$, G4-R(ZnO-QDs)$_{20}$, and G4-R(ZnO-QDs)$_{40}$. Scheme 1 depicts the ZnO-QDs @ bis MPA polyester-64-hydroxyl dendrimer synthesis scheme.

The ZnO-QDs @ bis MPA polyester-64-hydroxyl dendrimer nanostructures were characterized by UV-vis-NIR spectroscopy, Attenuated Total Reflectance Fourier Transform Infrared Spectroscopy (ATR-FTIR), Dynamic Light Scattering (DLS), Atomic force microscopy (AFM) and Raman spectroscopy.

Instrumental methods. The absorbance of nanostructures in water was measured using a Jasco v-670 UV-vis-NIR spectrophotometer. Experimental data were processed using the Spectra Measurement software. Dynamic light scattering experiments were conducted using a Malvern Zetasizer Nano ZS instrument in quartz cuvettes at 25 °C using the following parameters: a medium dispersion viscosity of 0.8872 mPa s, a solvent refractive index (RI) of 1.33, a material (ZnO) RI of 1.33. Experimental data were processed using the Zetasizer software.
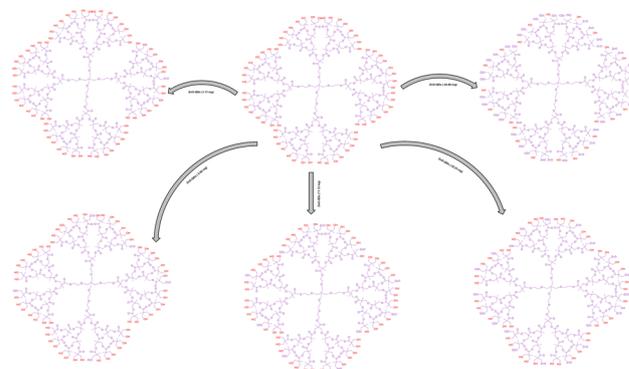
Scheme 1 Synthesis of ZnO-QDs @ bis MPA polyester-64-hydroxyl dendrimers.

AFM studies were performed using a Bruker Multimode 8 AFM probe microscope with a Nanoscope Bruker controller operating in the tapping mode. Experimental data were processed with a tip and cantilever using the following parameters: the material of the AFM cantilever: silicon nitride; tip radius: 6 nm; geometry: triangular; length: 120 μm; force constant: 0.35 N m^{-1}, and resonance frequency: 65 KHz using the NanoScope Analysis 1.4 software. FTIR spectra were measured using a Bruker/Alpha E Attenuated Total Reflectance Fourier Transform Infrared Spectrometer (ATR-FTIR). Raman spectra were measured using a Renishaw InVia Raman Microscope. Experimental data were processed using Wire 5.3.

Antimicrobial activity of ZnO-QDs @ bis MPA polyester-64-hydroxyl dendrimer nanostructures against *E. coli* and *S. aureus*. The Kirby Bauer Disk Diffusion assay was performed by setting up the stock culture of *S. aureus* (ATCC 25923) and *E. coli* (ATCC 25922) for the antimicrobial disks. The medium used in this test has to be the nutrient agar because it is an agar that is thoroughly tested for its composition and its pH level. The agar should be 4 mm deep. This further ensures standardization and reproducibility. For investigation of antimicrobial activity of the ZnO-QDs @ bis MPA polyester-64-hydroxyl dendrimer nanostructure solution against *E. coli* and *S. aureus*, the Kirby–Bauer Disk Diffusion assay was performed.[19] Nutrient agar (NA) media plates were prepared and 100 μl of the bacterial suspension was finely spread using a sterile glass spreader. Then ZnO-QDs @ bis MPA polyester-64-hydroxyl dendrimer nanostructures loaded on a disk of 5 mm diameter were placed in the centre of the medium using a sterile micropipette tip. The disk contains 10 μl of the ZnO-QDs @ bis MPA polyester-64-hydroxyl dendrimer nanostructure solution of 50 μg μl^{-1} concentration. The plates were incubated at 37 °C for 24 h. Subsequently, the zone of inhibition was observed in the plate and the diameter was measured on a milli meter-scale to study the antimicrobial activity. The assay was conducted in triplicate and the data are shown as the mean ± standard deviation (SD). Also, using this agar ensures that zones of inhibitions can be reproduced from the same organism.

Determination of the inhibitory concentration of 50% (IC$_{50\%}$) and 90% (IC$_{90\%}$) of the microorganisms. At least three replicates of three concentrations of each microorganism were used. The percentage inhibition was calculated using zone of inhibition data. The percentage inhibition values obtained were applied by using straight line equations to check the linearity of the method for each microorganism. The calculated data were shown in a scatter diagram that correlated the percentage inhibition with the concentrations of the antimicrobial agents used in the study. The "line of best fit" or "trend line" is formed in a scatter plot relatively close to almost all plot points. The squared correlation coefficient, or R^2, illustrates how closely the two variables in the scatter plot are related. A regression analysis of these data determines the best-fit line's equation to be Y = MX + C or Y = MX − C. To determine the IC$_{50\%}$ and IC$_{90\%}$, the derived equation was solved where X outcome was IC$_{50}$ and IC$_{90}$. The association between the concentration of antimicrobials and the % inhibition of the bacteria provided the value for "X" in the straight-line equations.

Notes

Green synthesis of colloidal zinc oxide quantum dots (ZnO-QDs)

Sono-chemistry was used to synthesize colloidal zinc oxide quantum dots (ZnO-QDs) *via* a controlled-precipitation approach. In a standard synthesis, 1.19 g of LiOH (≥98.0% Merck) was dissolved in 50 ml of pure methanol to make a 1 M lithium hydroxide solution, and 2.19 g of zinc acetate (98.0% SRL) was dissolved in 50 ml of pure methanol to make a 0.2 M zinc acetate solution. While stirring continuously, the LiOH solution was added dropwise to the zinc acetate solution until a pH value of 10 or 12 was attained. The reaction was then conducted for 3 hours at 45 to 50 degrees celsius in a 5 l Labman ultrasonic bath at 40 KHz and 150 W.[45] An esterification reaction between zinc acetate and methanol supports the generation of water and ester, as well as the growth of zinc oxide quantum dots. The pH value of the reaction solution during the synthesis was critical for the size of the quantum dots. More particularly, increasing pH values result in smaller quantum dots when keeping a constant synthesis time. The created quantum dots were cleaned by extracting them with hexane and heptane. Therefore, unreacted byproducts can be eliminated. Consequently, the supernatant was removed; the precipitated zinc oxide quantum dots were redistributed in ethanol and collected for storage and detailed analysis.[45]

X-ray diffraction (XRD) analysis. As a non-destructive method, X-ray diffraction (XRD) technology can be used to determine the crystallographic structure and phases of materials. The standard database can be used to identify the material and its phase for X-ray powder diffraction in large quantities of crystalline samples. XRD results indicate that ZnO-QDs were synthesized[45,54] Fig. 9 depicts the X-ray diffraction pattern of ZnO quantum dots. Powder XRD (PXRD) was used to identify ZnO-QDs and analyse their properties (Model: Bruker AXS D8 Focus P-XRD) with the following parameters: steps = 1407; time: 1 h 30 min; 2θ: 10 to 80°. The crystallite size can also be determined from the XRD spectrum pattern using the Origin pro 8.5 software and the Scherrer equation:
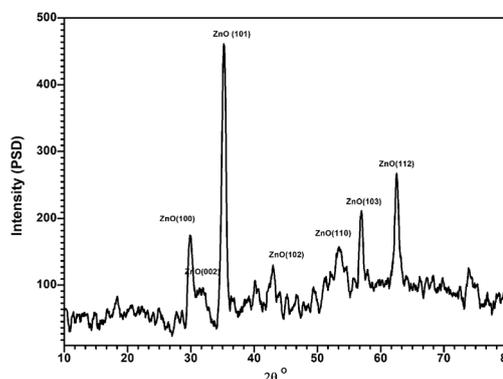
$$D = K\lambda / \beta \cos \theta$$

Fig. 9 X-ray diffraction pattern of ZnO quantum dots.

where D is the crystallite size (average in Å), K is the Scherrer constant with a value of 0.89 for spherical shape, λ is the wavelength of radiation and θ is the Bragg angle or diffraction angle of the peak. The FWHM values represent the full width at half maximum of the peaks. It was discovered that the diameter was 8 nm with a standard deviation of 2. The ESI file† contains exhaustive information of the X-ray diffraction (XRD) instrument parameters and calculation data. As a result, it is possible to infer characterization of ZnO-QDs from the DLS, UV-visible spectroscopy, and XRD characterization results. The ZnO-QDs have a radius of about 7 nm according to the powder X-ray diffraction profile of ZnO quantum dots.

Conclusions

This study successfully synthesized five novel ZnO-QDs @ bis MPA polyester-64-hydroxyl dendrimer nanostructures, which exhibited an increased surface area, thereby providing stability to the zinc oxide quantum dots and preserving the nano-scale size of the ZnO-QDs @ bis MPA polyester-64-hydroxyl dendrimer nanostructures. The bis MPA polyester-64-hydroxyl dendrimer had different numbers of surface functional groups functionalized by zinc oxide quantum dots. The five different bis MPA polyester-64-hydroxyl dendrimers were synthesized and analysed, with each functionalization having 1, 5, 10, 20 and 40 surface functional groups per bis MPA polyester-64-hydroxyl dendrimer. This study demonstrated that the degree of zinc oxide quantum dot functionalization influenced the chemical composition, characteristics and physical properties of each ZnO-QDs @ bis MPA polyester-64-hydroxyl dendrimer nanostructure. This nanostructure established the effect of multivalent functionalization levels on the properties and applications. The antibacterial effect of the ZnO-QDs @ bis MPA polyester-64-hydroxyl dendrimer nanostructures was investigated. The G4-R(ZnO-QDs)$_{10}$, G4-R(ZnO-QDs)$_{20}$, and G4-R(ZnO-QDs)$_{40}$ dendrimer nanostructures are effective *S. aureus* inhibitors, and the results were IC$_{50}$ values of 1099.56 µg µl^{-1}, 549.38 µg µl^{-1} and 282.31 µg µl^{-1} and IC$_{90}$ values of 1969.13 µg µl^{-1}, 979.95 µg µl^{-1} and 502.33 µg µl^{-1} respectively. According to the results, the nanostructure can be used for topical preparations such as creams or ointments for skin diseases. Based on the IC$_{50}$ and IC$_{90}$ values, the nanostructures can be utilized for water filtration, bandages, food packaging, surface coating, and reducing waterborne skin diseases.

Data availability

All data are available in the manuscript. The data supporting the XRD analysis in this manuscript are included as a part of the ESI file.†

Author contributions

First author and corresponding author Archana Zala designed study conception, and performed data collection, analysis, interpretation of the results and drafting of the manuscript. Co-Author Harshad Patel supervised the project. Both authors Archana Zala and Harshad Patel contributed to the final version of the manuscript. Both authors approved this version of the manuscript to be published. The authors declare no competing financial interest.

Conflicts of interest

There are no conflicts to declare.

References

1 S. K. Misra, H. H. Chang, P. Mukherjee, S. Tiwari, A. Ohoka and D. Pan, *Sci. Rep.*, 2015, **5**, 1–13.

2 E. Y. Furuya and F. D. Lowy, *Nat. Rev. Microbiol.*, 2006, **4**(1), 36–45.

3 T. Häusler, *Viruses vs. Superbugs*, Palgrave Macmillan, a division of Nature America Inc., 2006, DOI: **10.1007/978-0-230-55228-9**.

4 T. Naimi, P. Ringwald, R. Besser, S. Thompson and D. Bell, *Emerging Infect. Dis.*, 2001, **7**, 548.

5 J. S. Edwards, L. Betts, M. L. Frazier, R. M. Pollet, S. M. Kwong, W. G. Walton, W. K. Ballentine, J. J. Huang, S. Habibi, M. Del Campo, J. L. Meier, P. B. Dervan, N. Firth and M. R. Redinbo, *Proc. Natl. Acad. Sci. U. S. A.*, 2013, **110**, 2804–2809.

6 G. S. Lowell and R. S. Daum, in *Principles and Practice of Pediatric Infectious Disease*, 3rd edn, 2009, pp. 679–693.

7 A. Kérouanton, J. A. Hennekinne, C. Letertre, L. Petit, O. Chesneau, A. Brisabois and M. L. De Buyser, *Int. J. Food Microbiol.*, 2007, **115**, 369–375.

8 X. Yan, B. Wang, X. Tao, Q. Hu, Z. Cui, J. Zhang, Y. Lin, Y. You, X. Shi and H. Grundmann, *Appl. Environ. Microbiol.*, 2012, **78**, 6637–6642.

9 H. Y. Kim, J. A. Wiles, Q. Wang, G. C. G. Pais, E. Lucien, A. Hashimoto, D. M. Nelson, J. A. Thanassi, S. D. Podos, M. Deshpande, M. J. Pucci and B. J. Bradbury, *J. Med. Chem.*, 2011, **54**, 3268–3282.

10 W. Cheng, T. Xu, L. Cui, Z. Xue, J. Liu, R. Yang, S. Qin and Y. Guo, *J. Med. Chem.*, 2023, **66**, 962–975.

11 R. Yang, E. Hou, W. Cheng, X. Yan, T. Zhang, S. Li, H. Yao, J. Liu and Y. Guo, *J. Med. Chem.*, 2022, **65**, 16879–16892.

12 M. Otto, *Curr. Opin. Microbiol.*, 2014, **17**, 32–37.

13 J. C. Paton and A. W. Paton, *Clin. Microbiol. Rev.*, 1998, **11**, 450–479.

14 S. Bhakdi, N. Mackman, J. M. Nicaud and I. B. Holland, *Infect. Immun.*, 1986, **52**, 63–69.

15 A. Oliveira, C. Dias, R. Oliveira, C. Almeida, P. Fuciños, S. Sillankorva and H. Oliveira, *Crit. Rev. Microbiol.*, 2024, **50**(1), 87–104.

16 J. Qin, Y. Cui, X. Zhao, H. Rohde, T. Liang, M. Wolters, D. Li, C. B. Campos, M. Christner, Y. Song and R. Yang, *J. Clin. Microbiol.*, 2011, **49**, 3439–3440.

17 J. Sabota, *Am. J. Gastroenterol.*, 1998, **93**, 118–119.

18 V. J. Boyle, M. E. Fancher and R. W. Ross, *Antimicrob. Agents Chemother.*, 1973, **3**, 418–424.

19 K. R. Fiebelkorn, S. A. Crawford, M. L. McElmeel and J. H. Jorgensen, *J. Clin. Microbiol.*, 2003, **41**, 4740–4744.

20 W. L. Drew, A. L. Barry, R. O'Toole and J. C. Sherris, *Appl. Microbiol.*, 1972, **24**, 240–247.

21 A. Zala and H. Patel, *Appl. Microbiol.*, 2022, **20**, 1–13.

22 S. Saidin, M. A. Jumat, N. A. A. Mohd Amin and A. S. Saleh Al-Hammadi, *Mater. Sci. Eng., C*, 2021, **118**, 111382.

23 A. Verma, A. Singh, N. Shukla, S. K. Samanta and A. K. Sahoo, *Appl. Phys. A: Mater. Sci. Process.*, 2022, **128**, 1–10.

24 J. S. Kim, E. Kuk, K. N. Yu, J. H. Kim, S. J. Park, H. J. Lee, S. H. Kim, Y. K. Park, Y. H. Park, C. Y. Hwang, Y. K. Kim, Y. S. Lee, D. H. Jeong and M. H. Cho, *Appl. Phys. A: Mater. Sci. Process.*, 2007, **3**, 95–101.

25 S. Gurunathan, Y. J. Choi and J. H. Kim, *Int. J. Mol. Sci.*, 2018, **19**, 1210.

26 K. Mijnendonckx, N. Leys, J. Mahillon, S. Silver and R. Van Houdt, *BioMetals*, 2013, **26**, 609–621.

27 K. B. Riaz Ahmed, A. M. Nagy, R. P. Brown, Q. Zhang, S. G. Malghan and P. L. Goering, *Toxicol. Vitro*, 2017, **38**, 179–192.

28 K. Zheng, M. I. Setyawati, D. T. Leong and J. Xie, *ACS Nano*, 2017, **11**, 6904–6910.

29 C. Tao, *Lett. Appl. Microbiol.*, 2018, **67**, 537–543.

30 A. Rai, A. Prabhune and C. C. Perry, *J. Mater. Chem.*, 2010, **20**, 6789–6798.

31 M. Thripuranthaka, D. J. Late and S. S. Shinde, *JSM Nanomed. Nanotechnol.*, 2015, **3**, 1033.

32 N. Padmavathy and R. Vijayaraghavan, *Sci. Technol. Adv. Mater.*, 2008, **9**, 35004–35011.

33 A. C. Janaki, E. Sailatha and S. Gunasekaran, *Spectrochim. Acta, Part A*, 2015, **144**, 17–22.

34 R. Kumar, A. Umar, G. Kumar and H. S. Nalwa, *Ceram. Int.*, 2017, **43**, 3940–3961.

35 M. Arakha, M. Saleem, B. C. Mallick and S. Jha, *Sci. Rep.*, 2015, **5**, 1–10.

36 M. S. Usman, M. E. El Zowalaty, K. Shameli, N. Zainuddin, M. Salama and N. A. Ibrahim, *Int. J. Nanomed.*, 2013, **8**, 4467–4479.

37 J. Ramyadevi, K. Jeyasubramanian, A. Marikani, G. Rajakumar and A. A. Rahuman, *Mater. Lett.*, 2012, **71**, 114–116.

38 L. de, A. S. de Toledo, H. C. Rosseto and M. L. Bruschi, *Pharm. Dev. Technol.*, 2018, **23**, 316–323.

39 M. Arakha, S. Pal, D. Samantarrai, T. K. Panigrahi, B. C. Mallick, K. Pramanik, B. Mallick and S. Jha, *Sci. Rep.*, 2015, **5**, 1–12.

40 Y. Vitta, M. Figueroa, M. Calderon and C. Ciangherotti, *Mater. Sci. Energy Technol.*, 2020, **3**, 97–103.

41 K. Gold, B. Slay, M. Knackstedt and A. K. Gaharwar, *Adv. Ther.*, 2018, **1**(3), 1700033.

42 P. Joshi, S. Chakraborti, P. Chakrabarti, D. Haranath, V. Shanker, Z. A. Ansari, S. P. Singh and V. Gupta, *J. Nanosci. Nanotechnol.*, 2009, **9**, 6427–6433.

43 T. Jin, D. Sun, J. Y. Su, H. Zhang and H. J. Sue, *J. Food Sci.*, 2009, **74**, M46–M52.

44 V. Muşat, A. Tabacaru, B. Ş. Vasile and V. A. Surdu, *RSC Adv.*, 2014, **4**, 63128–63136.

45 W. Yang, B. Zhang, N. Ding, W. Ding, L. Wang, M. Yu and Q. Zhang, *Ultrason. Sonochem.*, 2016, **30**, 103–112.

46 W. Yang, B. Zhang, N. Ding, W. Ding, L. Wang, M. Yu and Q. Zhang, *Ultrason. Sonochem.*, 2016, **30**, 103–112.

47 S. J. Yang and C. R. Park, *Nanotechnology*, 2008, **19**, 4.

48 W. Yang, H. Yang, W. Ding, B. Zhang, L. Zhang, L. Wang, M. Yu and Q. Zhang, *Ultrason. Sonochem.*, 2016, **33**, 106–117.

49 C. P. Prasanth, E. Joseph, A. Abhijith, D. S. Nair, I. Ibnusaud, J. Raskatov and B. Singaram, *J. Org. Chem.*, 2018, **83**, 1431–1440.

50 J. Grobelny, F. W. DelRio, N. Pradeep, D. I. Kim, V. A. Hackley and R. F. Cook, in *Methods in Molecular Biology*, Humana Press, 2011, vol. 697, pp. 71–82.

51 A. Sirelkhatim, S. Mahmud, A. Seeni, N. H. M. Kaus, L. C. Ann, S. K. M. Bakhori, H. Hasan and D. Mohamad, *Nano-Micro Lett.*, 2015, **7**, 219–242.

52 X. Zhang, Y. Dai and G. Dai, *Polym. Chem.*, 2020, **11**, 964–973.

53 C. Deraedt, R. Ye, W. T. Ralston, F. D. Toste and G. A. Somorjai, *J. Am. Chem. Soc.*, 2017, **139**, 18084–18092.

54 B. Qiao, S. Zhao, Z. Xu and X. Xu, *Chin. Phys. B*, 2016, **25**(9), 098102.